

Insulating Ag–Polyimide Hybrid Films with a Tunable Dielectric Constant


Markus Klaus Diether Wiesinger,* Till Welzel, and Martin Stutzmann*

Herein, the production of nonpercolative hybrid insulating films with adjustable dielectric constant at low filler fractions is reported. These films might be useful to shape field distributions in passivation stacks or as dielectrics in passive components of integrated circuits such as capacitors. It is shown how such a system can be realized with commercially available materials and simple tools and how they can be significantly improved by adapting the processing techniques applied. The improved electric and dielectric properties are related to changes in the microstructure of the films caused by the different processing conditions. The experiments show that the films possess sufficiently stable properties from room temperature up to 150 °C, which enable them to be used in devices. Finally, a model is proposed for the dielectric breakdown of the films that gives a direction for the further improvement of such material systems.

1. Introduction

Hybrid dielectric polymers have recently attracted interest in the scientific community, e.g., as new dielectric materials, for use as dielectrics in various capacitors, e.g., as passive components^[1–4] or in energy storage systems^[5,6] or as screening layers for microwaves.^[7] While pristine dielectric polymers offer many advantages, such as low-cost processing, flexibility, and low-temperature processes, they suffer from generally a low dielectric constant. Hybrid polymers should overcome this issue by having an increased dielectric constant while maintaining the benefits from polymers. This can be achieved for instance when ceramics with a high dielectric constant, like $\text{CaCu}_3\text{TiO}_4\text{O}_{12}$ ^[7–10] or BaTiO_3 ,^[6,11] are embedded in a polymer matrix to increase the effective dielectric constant of the overall film. This approach is usually limited by the high filler fraction needed for noticeable effects, which might significantly alter the beneficial properties of the polymer (e.g., flexibility). Another approach is to utilize

M. K. D. Wiesinger, T. Welzel, Prof. M. Stutzmann
Walter Schottky Institute and Physics Department
Technical University Munich
Am Coulombwall 4a, Garching 85748, Germany
E-mail: markus.wiesinger@wsi.tum.de; stutz@wsi.tum.de

 The ORCID identification number(s) for the author(s) of this article can be found under <https://doi.org/10.1002/pssa.201900488>.

© 2019 The Authors. Published by WILEY-VCH Verlag GmbH & Co. KGaA, Weinheim. This is an open access article under the terms of the Creative Commons Attribution-NonCommercial License, which permits use, distribution and reproduction in any medium, provided the original work is properly cited and is not used for commercial purposes.

DOI: 10.1002/pssa.201900488

interfacial polarization, which occurs when mixing (semi)conductive particles into a nonconductive matrix. When increasing the filler fraction of the conductor up to just before the insulator–conductor transition, the dielectric constant diverges with a power-law dependence, which is described by the percolation theory. This has already been utilized several times^[1,2,12,13] but has intrinsic technological problems: first, the transition described by percolation always includes a power-law increase in the conductivity aside the power-law divergence of the dielectric constant.^[14,15] Second, the power-law divergence itself is a problem, as usually very small fluctuations of the filler content can significantly change the electric and dielectric properties

of the material in the region of interest. Hence, percolation might be a suitable approach for screening layers, where an increased conductivity at low filler fraction is not detrimental but not the preferred approach to produce insulating materials. However, a different approach is explored in this work. We use conductive Ag nanoparticles (NPs) that are covered with an insulating layer of polyvinylpyrrolidone (PVP) to prevent percolation effects. In a similar system of Ag NPs in poly(vinylidene fluoride),^[16,17] it has already been shown that the presence of the NPs can change the polymer phase produced, which goes beyond this work. The Ag NPs are incorporated into a polyimide (PI) matrix, because PI is known for its excellent thermal and mechanical stability and is widely used in commercial devices. The effect of the polarization at the internal conductor–dielectric interfaces on the dielectric and electric properties of the effective medium was first described by Maxwell, Wagner, and Sillars^[9,18,19] and should in first order only depend linearly on two parameters: the conductivity of the filler and the filler content, if percolation is suppressed. In this article, we will focus on the production and characterization of thin dielectric films (<1 μm) and on how different production techniques can change the properties of our material system, and we will relate this to the produced microstructures. To the best of our knowledge, these points have hardly been addressed in the literature so far.

2. Results and Discussion

2.1. NP and Hybrid Film Morphology

To check the quality of NP dispersion and understand the effects that the different process versions “us” versus “ann-us” have on

our samples, we drop casted the pure NP dispersion without the polymer on a substrate. The scanning electron microscopy (SEM) images of the resulting NP films are shown in **Figure 1a,b**. The images show that the “us” NPs are almost spherical with an average diameter that agrees with the value provided by the supplier. For the “ann-us” NPs, the SEM image shows larger structures that can be explained by sintering of the NPs. We have annealed at a temperature within the range of the glass transition temperature of the PVP shell.^[20] Hence, it is likely that the NP shells fused together forming larger, nonspherical particles. We have measured the film thickness and roughness of the hybrid PI–NP films and plotted them for each investigated structure versus the Ag filler fraction (**Figure 1c,d**). The data show an increase in film thickness and root mean square (rms) roughness for higher Ag content that can be explained by a higher viscosity of the dispersion and clustering of NPs in the film. For an unknown reason, the 2.5 vol% “us-PI” films fall out of that general trend. The “ann-us-PI” films exhibit an overall lower surface roughness compared with the “us-PI” films as well as less scattering of the data points, especially for higher filler fractions. Furthermore, low loading with “ann-us” NPs (<7.5%) has an almost negligible effect on film thickness. Altogether, this indicates that “ann-us” NPs are better incorporated into the polymer film than the “us” NPs. To support this hypothesis, we have checked the morphology of our hybrid films with optical and electron microscopy. In **Figure 2**, we show representative microscope images for “us-PI” (a–c) and “ann-us-PI” (d–e) films for three different NP concentrations. In the “us” samples, the NPs form large agglomerates inside the film that are visibly as black spots. With increasing NP concentration (a–c), the cluster size increases and the clusters begin to connect. For each

concentration, the size of the agglomerates for the “ann-us-PI” samples is smaller than for the “us” samples. Furthermore, the distribution of the particles looks more homogeneous as there are fewer large agglomerates, and they are more evenly distributed over the sample and do not form clearly visible networks of particles.

To verify this result on a microscopic scale, SEM measurements have been performed. The SEM images shown in **Figure 3** are captured at the edges of scratches that have been cut into the film next to the electrical contacts to provide a zero line for the profilometer and allow us, therefore, to also see the lateral distribution of NPs inside the film with the SEM. As we operate the SEM at rather low voltages and use an in-lens detector, the electrons detected are mainly the ones that undergo elastic Coulomb scattering close to the surface. Hence, we are sensitive to the morphology as well as to the charge distribution at the surface of the film, as Coulomb scattering is proportional to the charge in the scattering particles. The pictures show that grape-like structures are embedded in the otherwise smooth polymer film. We attribute these structures to the Ag–NP clusters. With increasing Ag content, the amount of clusters and their size increases for the “us-PI” (**Figure 3a–c**) and the “ann-us-PI” films (**Figure 3d–f**). The more evenly distributed NPs in the “ann-us” films are most obvious for highest and lowest filler fractions. For the lowest filler fraction, one can see typical cluster structures in the upper part of **Figure 3a**, which are several micrometers long. The “ann-us” sample shows in total more clusters, which are typically in the range of few hundreds of nanometers up to 1 μm . For the highest NP concentration, it is more instructive to look at the areas between the clusters: for the “us” samples, there are few but large spots of flat polymers in

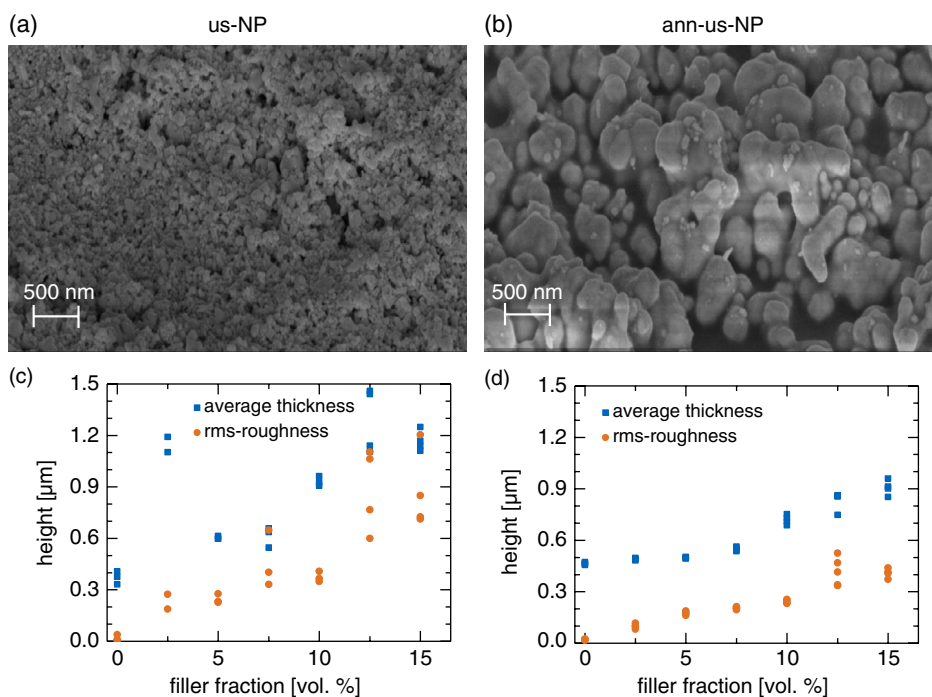


Figure 1. SEM micrographs of drop-casted films prepared from a) ultrasonicated and b) annealed Ag nanoparticles. c,d) Film thickness and rms roughness of the corresponding hybrid films plotted for each capacitor versus the volume fraction of Ag in the film.

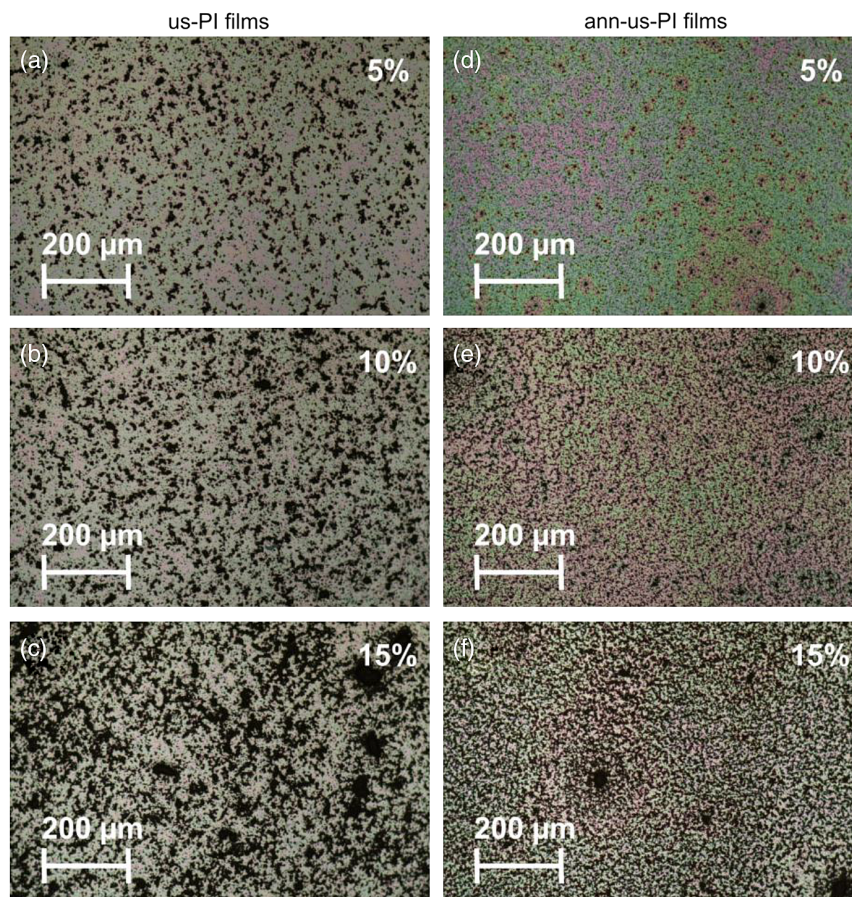


Figure 2. Optical micrographs of hybrid films containing a, d) 5 vol%, b, e) 10 vol%, and c, f) 15 vol% Ag nanoparticles. The samples in (a–c) are the us-PI films, whereas (d–f) are the ann-us films.

between the NP clusters, whereas for the “ann-us” samples, there are more but much smaller flat regions separating the smaller agglomerates. Altogether, the measurements indicate that the bigger “ann-us” particles are dispersed better in the PI and form a more homogeneous film. This behavior can be explained via a change in the interface energy of the PI–NP interface when the NPs are annealed. This is supported by contact angle measurements not shown here.^[21] The polymer, we use, already consists of rather long chains and therefore might not form a low energy interface with the small NPs. When the NPs sinter during annealing and form larger particles, this leads to a change in interaction between NP and polymer chains and therefore reduces the surface energy and the clustering of NPs in the film. This indicates that we can significantly improve the morphology of our films and more precisely, the NP incorporation in the film just by simply annealing the NPs prior to mixing them into the film.

2.2. Electric and Dielectric Properties

To quantify the influence of the film morphology on the electrical characteristics, we performed impedance measurements on our samples. For the “us” samples (Figure 4a), the real part of the

dielectric function increases with the filler fraction over the investigated frequency range. For higher filler fractions, the deviations between the single samples increase rapidly, which causes the error bars to increase. We only plotted two error bars per concentration for these samples for reasons of clarity. If we look at the evolution of the real part of the dielectric function versus the filler fraction (Figure 4b), we see that within our measurement range there is a linear dependence of ϵ_1 on filler fraction. 3D percolation for spherical particles should lead to a percolation threshold of around 16 vol%,^[15,22–24] depending on the model and, therefore, to a divergence of the real part of the dielectric function at or before that filler fraction. Nonspherical particle shape, clustering or strong particle–particle interaction as observed here, should decrease this value as already shown in the literature.^[22,25] Hence, we state that we see no sign of percolation or electrode polarization in the real part of the dielectric function, as expected for systems with an isolating shell around each NP. To validate this, we determined the loss tangent and the conductivity for our samples (Figure 4c,d). The loss factor shows two distinct features: an increase at high frequencies independent of the NP filler fraction and an increase at low frequencies for higher filler fractions with a maximum between 5 and 10 vol%. The high-frequency behavior can be explained by the series resistance

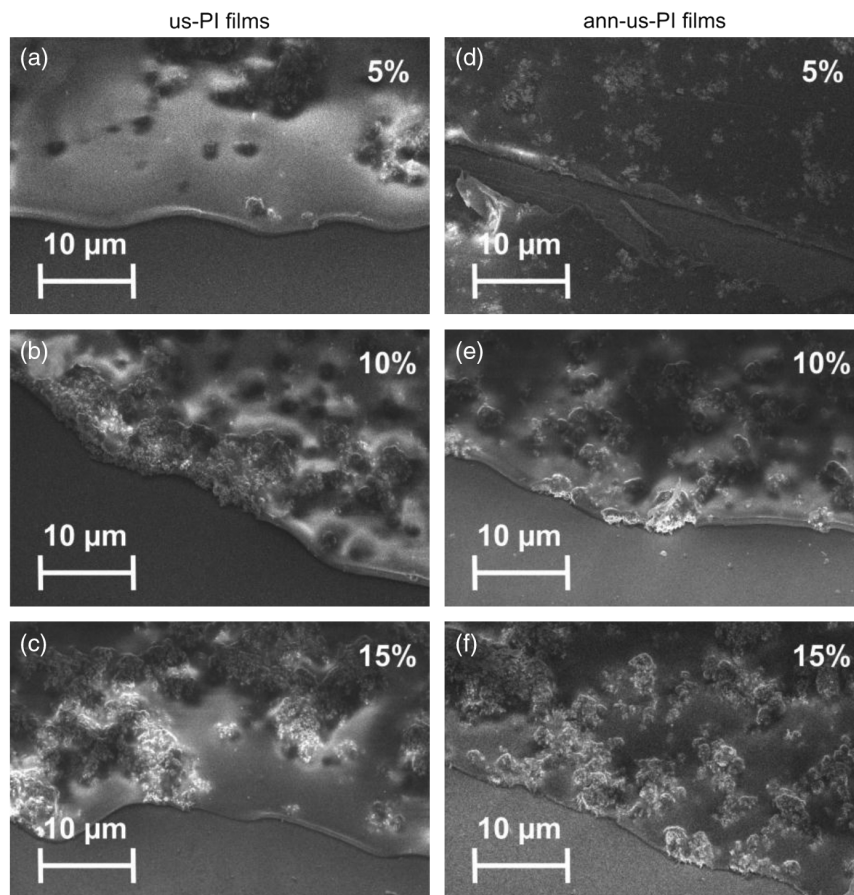


Figure 3. SEM images of the samples. a,d) 5 vol%, b,e) 10 vol%, and c,f) 15 vol% Ag nanoparticles. The samples in (a–c) are the us-PI films, whereas (d–f) are the ann-us films.

from our back electrode and setup that we cannot account for precisely, whereas the low-frequency component indicates some charge transfer in our film that becomes more dominant at low frequencies. The maximum for both the low-frequency loss factor and DC conductivity are due to a too large sample-to-sample variation in the raw data, which is supported by large error bars for the loss factor. The cause for this could be an insufficient dispersion quality originating from different local deviations in the “us” power, insufficient control over the mixing between PI and NP dispersion or the manual spin coating. The change in conductivity supports this conclusion, as the DC conductivity changes by 2.5 orders of magnitude with increasing NP filler fraction, whereas the alternating current (AC) conductivity at 100 kHz changes less than one order of magnitude (Figure 4d). Nevertheless, the increase in DC conductivity is far less than expected for a percolative system. Furthermore, measurements with finger structures covered with films of pure “us” and “ann-us” NPs (drop casted on the prefabricated finger structures on SiO₂) indicate a conductivity of the order of 10⁻⁷ and 10⁻⁶ Ω⁻¹ cm⁻¹, respectively. This implies that the DC conductivity of our films is influenced but not dominated by the conductivity of the NPs, yet. The same measurements have been performed on the “ann-us” samples [Figure 5]. The more homogeneous morphology results in fewer deviations in the

electrical properties and leads to reduced error bars and a clearer trend of the frequency-dependent real part of the dielectric function. Again, we see a linear trend of the real part of the dielectric function. At 15 vol%, the real part of the dielectric function is higher than the linear trend of the other samples, which could be a sign for the onset of percolation. A clear difference between “us” and “ann-us” samples is shown in the low-frequency loss tangent and conductivity, which are lower for the “ann-us” samples than for the “us” samples, as discussed in the later sections. While there is still a small influence of the filler fraction on the low-frequency loss tangent for the “ann-us” samples (see inset in Figure 5c), the strong increase seen for the “us” samples completely vanishes via annealing. Furthermore, the DC conductivity decreases by almost one order of magnitude for the highest filler fraction compared with the “us” samples. This indicates that although the “us” samples already show an adjustable dielectric constant, annealing improves the electric properties of the material by, on the one hand, reducing the DC conductivity and low-frequency loss tangent and, on the other side, by making the electric properties more predictable. In both cases, the PVP shell of the Ag nanoparticles is able to suppress percolation effects in both the dielectric constant and the conductivity of the samples.

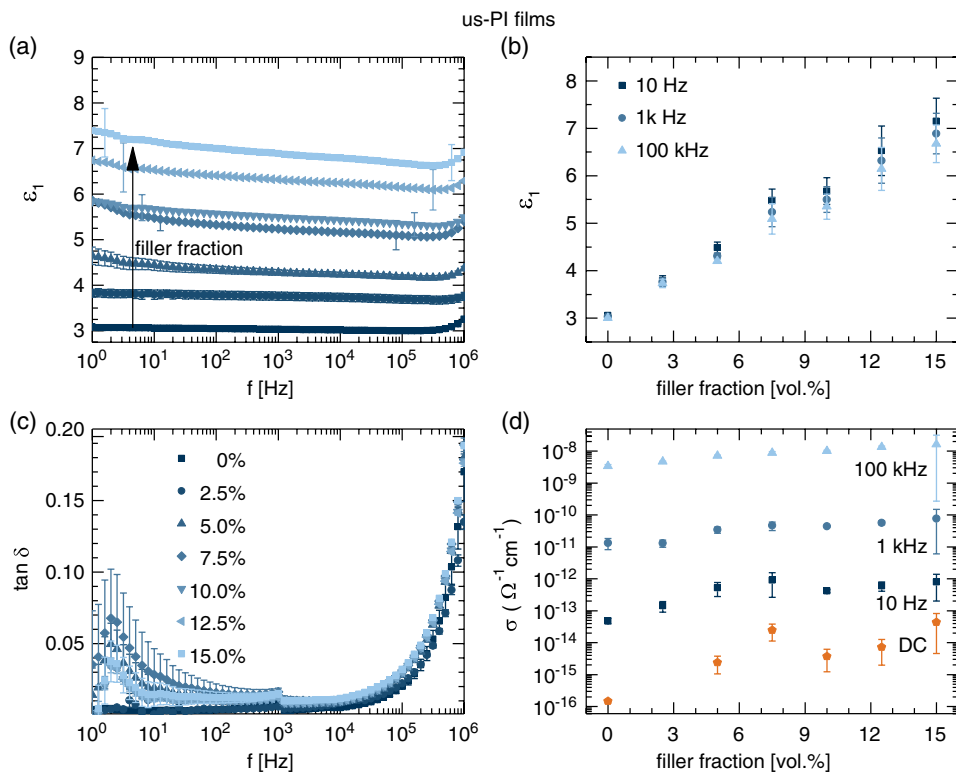


Figure 4. a) The real part of the dielectric function and c) loss factor plotted versus frequency of hybrid films made with filler fractions ranging from 0 to 15 vol% of ultrasonicated nanoparticles. b) Real part of the dielectric function and d) conductivity versus filler fraction for different frequencies.

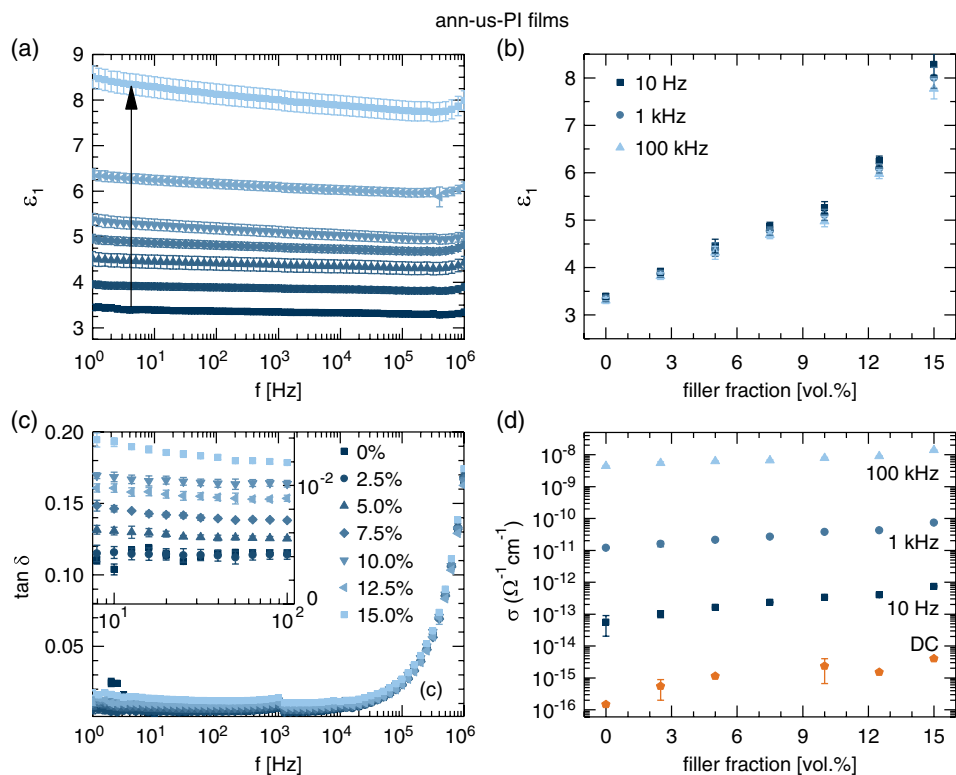


Figure 5. a) Real part of the dielectric function and c) loss factor versus frequency of hybrid films made with different filler fractions of annealed nanoparticles. b) Real part of the dielectric function and d) conductivity plotted versus filler fraction for different frequencies.

2.3. Temperature Stability

For the application of a new material in a device, either as part of a passive or active component, its properties have to be sufficiently stable in the temperature range of operation. To show this, we measured the dielectric and electric properties for temperatures between room temperature and 150 °C (Figure 6). As samples, we chose the best-performing samples with the lowest loss tangent and conductivity for 10 vol% Ag NPs to have a measurable effect of the nanoparticles and compare the best cases for both processing methods. The real parts of the dielectric function of both samples increase with increasing temperature mainly in the low-frequency region by 7% and 5%, respectively. The loss factor shows an equivalent dependence

on the temperature but always stays below 0.05 for low frequencies. A more pronounced trend can be found in the DC conductivity. The DC conductivity of the “ann-us” samples always stays below that of the “us” samples as in the previous experiment, and both samples stay insulating. In an Arrhenius plot, the data points for both samples do not lie on straight lines (Figure 6e). Hence, we cannot explain this data by a single thermally activated process. Due to the limited temperature range, fitting two activation energies is possible but the result would remain questionable. Overall, the properties of our samples, in particular, the real part of the dielectric function and conductivity, are sufficiently temperature stable, with the “ann-us” samples again outperforming the “us” samples.

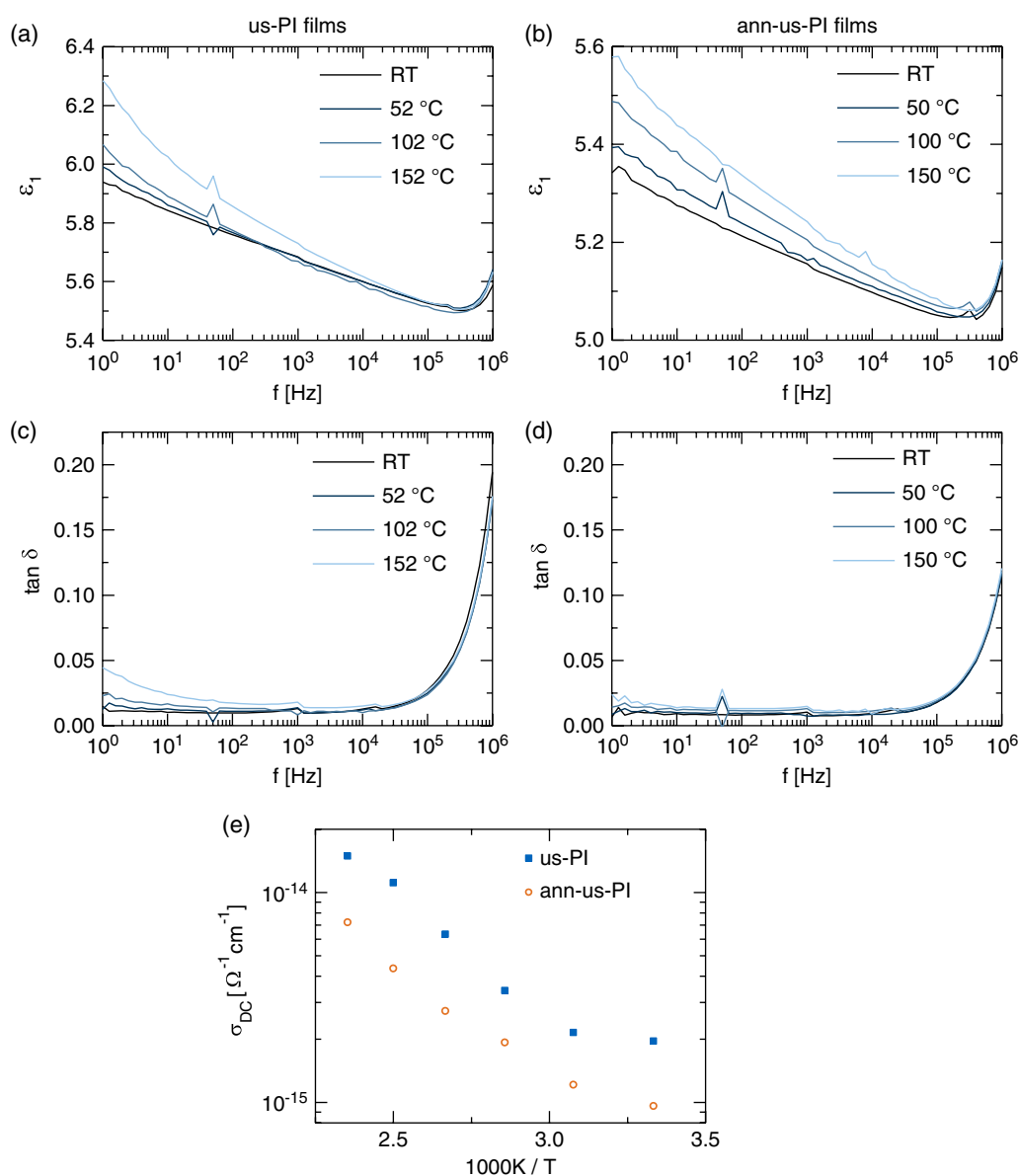


Figure 6. a,b) Real part of the dielectric function and c,d) loss factor versus frequency of a hybrid film containing 10 vol% a,c) us-NPs or b,d) ann-us-NPs measured at different temperatures. e) The DC conductivity versus temperature for both samples shown in (a–d).

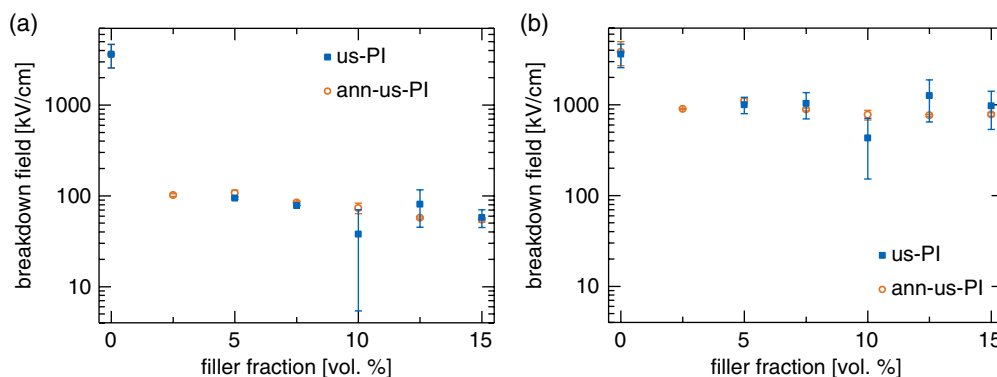


Figure 7. Breakdown field for hybrid films containing different filler fractions of ultrasonicated or annealed particles. a) The data calculated from the raw data. b) The data considering a procedure explained in Section 2.4.

2.4. Dielectric Breakdown

The last important property that we have investigated is the dielectric breakdown field. We measured the dielectric breakdown by monitoring the current while ramping up the voltage. The current abruptly increases at breakdown voltage, which we take to calculate the breakdown field (Figure 7). This measurement is destructive and was therefore performed last. If we calculate the breakdown field using the average film thickness, we obtain the plot shown in Figure 7a. The breakdown field abruptly decreases by more than one order of magnitude, when adding NPs. Afterwards, it only slightly decreases with increasing filler fraction. Within the error bars, there is no significant difference between differently processed NPs in this measurement. As we have a very inhomogeneous medium with varying thickness, using the average film thickness to calculate the breakdown field might not be reasonable. We propose a different model to calculate the dielectric breakdown field here: dielectric breakdown will happen at the points of the film that are exposed to the highest field. These are the points with the lowest thickness of the dielectric film in between the electrodes, as the voltage applied gives the potential drop. The weakest spot that one can imagine for our system is a thin region of the PI film next to a cluster of NPs, where only one has to break through the PVP shell of the NPs instead of the whole polymer film. To estimate the breakdown field for this case, we did not use the average but used the 10th percentile of the film thickness. Next, we calculated how many NPs arranged in a linear chain would give that film thickness and added their shell thicknesses together to obtain an effective dielectric thickness that has to withstand the electric field. This calculation leads to the breakdown field shown in Figure 7b. In this model, the breakdown field scatters around 1000 kV cm^{-1} for all samples containing NPs, which is comparable with the literature values for organic dielectrics.^[26] The scattering of our data can be explained by small local deviations in the microstructure from our model, like in the diameter or the linear chain of NPs. We see this as a strong argument that our breakdown field is limited only by the breakdown field of the PVP shell of our NPs that do not seem to be affected by processing. Measuring the breakdown field of the PVP shell of the NPs directly should have been the next step but was not possible.

Pure NP films were not dense or mechanically stable enough to perform electrical measurements on them. Hence, a direct comparison of the breakdown field of our hybrid films with the breakdown properties of our NPs itself is not possible at this point.

3. Conclusions

In summary, we could show that we can produce a low-cost hybrid spin-on dielectric with a tunable real part of the dielectric function. A proper choice of the materials used can prohibit percolation, although clustering of the NPs is still present. Adjusting the processing conditions can significantly improve the morphology of the resulting dielectric films. The optimized processing also increases the low frequency and especially the DC characteristics of our material. Furthermore, we proposed an explanation for our low breakdown fields. For further improvement of such materials, the remaining clustering should be suppressed to improve the breakdown voltage as an important material property.

4. Experimental Section

Materials: PVP-coated Ag NPs with a nominal diameter of $d < 100 \text{ nm}$ (purchased from Sigma Aldrich), *N*-methyl-2-pyrrolidone (NMP) (BASF, VLSI grade), and the PI Durimide 7920 (Fujifilm) were used as received. The PVP fraction of the Ag NPs was measured via thermal decomposition of the PVP shell and was found to be about 5 wt%. With this value, we calculated the thickness of the PVP shell to be 6.6 nm for a particle with a total diameter of 100 nm.

Sample Preparation: A weighted amount of NPs was predispersed in NMP. To improve the dispersion quality and break up soft agglomerates, visible with the naked eye, the mixture was either put into a 10°C cool ultrasound bath for 4 h (from here, referred to as “us” NPs or “us-PI” films) or annealed for 4 h at 135°C under constant stirring and ultrasonicated at 10°C for an additional hour afterward (referred to as “ann-us” NPs or “ann-us-PI” films). The resulting black-colored NP dispersion was mixed with the PI at room temperature in a 1:1 ratio via stirring, shaking, and ultrasonication until all visible streaks of the PI in the mixture disappeared.

As substrates for the films, $1.2 \times 1.2 \text{ cm}^2$ pieces of polished p-type silicon wafers with a specific resistivity of $1\text{--}20 \Omega\text{cm}$ were used. After thermally evaporating a 150 nm-thick aluminum back electrode in high vacuum, the samples were spin coated with the PI–NP mixture for 40 s at

4500 rpm. Afterward, they were soft baked for 3 min on a hotplate at 150 °C and crosslinked in a vacuum oven for 1 h at 350 °C. To prevent the remaining solvent to form gas bubbles during crosslinking, the temperature was changed with less than 10 °C min⁻¹. On top of each sample, we deposited four round top aluminum contacts with a diameter of 3 mm via thermally evaporating 150 nm of aluminum in high vacuum with a shadow mask covering parts of the sample. The back electrode was contacted after removing a small part of the PI film at one edge of the sample with a razor blade.

Measurements: The sample morphology was analyzed visually with an optical microscope. For higher-resolution images, we used the scanning electron function of a Zeiss NVision 40 SEM/FIB system. The scanning electron micrographs were recorded with the acceleration voltage of the electron beam set to 5 kV, and the in-lens detector was used for data acquisition while the sample was tilted by 45° with respect to the incident electron beam. Film thickness and roughness were measured at four spots around each contact with a Veeco Dektak 150 profilometer which produces 1D height profiles of 1 mm length. A scratch in the film next to the contact served as a reference height. The surface profiles were handled as a single dataset containing 30 000–35 000 data points for each contact. Electrical measurements were performed in a home-built thermostat, allowing low noise measurements in vacuum or under ambient conditions and at different temperatures. We performed impedance measurements using a Zurich instrument MFIA impedance analyzer and DC current–voltage measurements using a Keithley 6517B/E electrometer and a Keithley 2400 source-measure unit.

Acknowledgements

This work was supported by funding from TUM.solar in the context of the Bavarian Collaborative Research Project “Solar Technologies Go Hybrid” (SolTech) and Infineon Technologies AG.

Conflict of Interest

The authors declare no conflict of interest.

Keywords

composite materials, dielectrics, hybrid materials, nanoparticles

Received: June 24, 2019

Revised: October 9, 2019

Published online: November 11, 2019

- [1] M. Yang, H. Zhao, D. He, J. Bai, *Appl. Phys. Lett.* **2016**, *109*, 72906.
- [2] Y. Sun, J. Wang, S. Qi, G. Tian, D. Wu, *Appl. Phys. Lett.* **2015**, *107*, 12905.
- [3] X. Kuang, Z. Liu, H. Zhu, *J. Appl. Polym. Sci.* **2013**, *129*, 3411.
- [4] X. Huang, P. Jiang, L. Xie, *Appl. Phys. Lett.* **2009**, *95*, 242901.
- [5] S. Nasreen, M. L. Baczkowski, G. M. Treich, M. Tefferi, C. Anastasia, R. Ramprasad, Y. Cao, G. A. Sotzing, *Macromol. Rapid Commun.* **2019**, *40*, e1800679.
- [6] W. Sun, X. Lu, J. Jiang, X. Zhang, P. Hu, M. Li, Y. Lin, C.-W. Nan, Y. Shen, *J. Appl. Phys.* **2017**, *121*, 244101.
- [7] Y. Qing, Z. Yang, Q. Wen, F. Luo, *Appl. Phys. A* **2016**, *122*, 640.
- [8] Q. G. Chi, J. F. Dong, C. H. Zhang, C. P. Wong, X. Wang, Q. Q. Lei, *J. Mater. Chem. C* **2016**, *4*, 8179.
- [9] J. C. Maxwell, *A Treatise On Electricity & Magnetism*, Dover Publications, Inc., New York **1954**.
- [10] Y. Yang, B.-P. Zhu, Z.-H. Lu, Z.-Y. Wang, C.-L. Fei, D. Yin, R. Xiong, J. Shi, Q.-G. Chi, Q.-Q. Lei, *Appl. Phys. Lett.* **2013**, *102*, 42904.
- [11] K. Yang, X. Huang, Y. Huang, L. Xie, P. Jiang, *Chem. Mater.* **2013**, *25*, 2327.
- [12] J. Sun, Q. Xue, L. Chu, Q. Guo, T. Lei, F. Xia, Z. Zhang, *Polym. Compos.* **2016**, *37*, 327.
- [13] J.-Y. Kim, T. Kim, J. W. Suk, H. Chou, J.-H. Jang, J. H. Lee, I. N. Kholmanov, D. Akinwande, R. S. Ruoff, *Small* **2014**, *10*, 3405.
- [14] B. I. Shklovskii, A. L. Éfros, *Sov. Phys.-Usp.* **1975**, *18*, 401.
- [15] V. E. Dubrov, M. E. Levinshtein, M. S. Shur, *Sov. Phys. JETP* **1976**, *43*, 1050.
- [16] S. Manna, S. K. Batabyal, A. K. Nandi, *J. Phys. Chem. B* **2006**, *110*, 12318.
- [17] D. Mandal, K. Henkel, D. Schmeisser, *J. Phys. Chem. B* **2011**, *115*, 10567.
- [18] R. W. Sillars, *J. Inst. Electr. Eng.* **1937**, *80*, 378.
- [19] K. W. Wagner, *Arch. Elektrotech.* **1914**, *2*, 371.
- [20] M. del Pilar Buera, G. Levi, M. Karel, *Biotechnol. Prog.* **1992**, *8*, 144.
- [21] Contact angle was measured with water on drop casted films of “us” and “ann-us” NPs. While the contact angle was 0° for the “us” NPs, it increased to an average of 10° for the “ann-us” NPs.
- [22] C.-W. Nan, Y. Shen, J. Ma, *Annu. Rev. Mater. Res.* **2010**, *40*, 131.
- [23] B. I. Shklovskii, A. L. Éfros, *Sov. Phys.-Usp.* **1975**, *18*, 845.
- [24] D. M. Grannan, J. C. Garland, D. B. Tanner, *Phys. Rev. Lett.* **1981**, *46*, 375.
- [25] R. Schueler, J. Petermann, K. Schulte, H.-P. Wentzel, *J. Appl. Polym. Sci.* **1997**, *63*, 1741.
- [26] R. Ponce Ortiz, A. Facchetti, T. J. Marks, *Chem. Rev.* **2010**, *110*, 205.